Numerical studies on weak and strong ignition induced by reflected shock and boundary layer interaction

Chengyang Huang[1,2], Yuan Wang[3], Ralf Deiterding[4], Zheng Chen[1*]

[1] SKLTCS, HEDPS, CAPT, College of Engineering, Peking University, Beijing, China

[2] [黄成扬目前单位]

[3]Institute of Applied Physics and Computational Mathematics, Beijing 100094, China

[4]Aerodynamics and Flight Mechanics Research Group, University of Southampton, Highfield Campus, Southampton SO17 1BJ, United Kingdom

Abstract

In shock tube experiments, the interaction between the reflected shock and boundary layer can induce shock bifurcation and weak ignition. The weak ignition can greatly affect the ignition delay time measurement in a shock tube experiment. In this work, two-dimensional simulations considering detailed chemistry and transport are conducted to investigate the shock bifurcation and non-uniform ignition behind a reflected shock. The objectives are to interpret the formation of shock bifurcation induced by the reflected shock and boundary layer interaction, and to investigate the weak ignition and its transition to strong ignition for both hydrogen and dimethyl ether. It is found that the asynchronous reflection of the incident shock at the end wall produces a wedge-shaped oblique shock foot at the wall. The wedge-shaped structure results in strong interactions between reflected shock and boundary layer, which induces the shock bifurcation. It is demonstrated that the local high temperature spots at the foot of the bifurcated shock is caused by viscous dissipation and pressure work. As the post-reflected shock temperature increases, the transition from weak ignition to strong ignition in a stoichiometric hydrogen/oxygen mixture is observed. The relative sensitivity of ignition delay time to the post-reflected shock temperature is introduced to characterize the appearance of weak ignition behind the reflected shock. Unlike in the hydrogen/oxygen mixture, weak ignition is not observed in the stoichiometric dimethyl-ether/oxygen mixture since it has relatively longer ignition delay time and smaller relative sensitivity.

I. INTRODUCTION

A shock tube is popularly used to study the ignition and detonation properties of different fuels [1, 2]. The ignition delay time (IDT) measured in shock tube experiments is one of the main targets for kinetic model development and validation [1, 3]. In ideal shock tube experiments, homogeneous ignition is expected to occur in the region between the reflected shock and the end wall. Unfortunately, in practice non-uniform ignition might happen due to the asynchronous reflected-shock compression, shock attenuation, boundary layer growth, or the interaction between the reflected shock and boundary layer [4-7]. For example, the reflected shock and boundary layer interaction can result in shock bifurcation, which may induce local ignition and increase the error in IDT measurements [5, 8-11]. In this study, the non-uniform ignition caused by the reflected shock and boundary layer interaction is investigated.

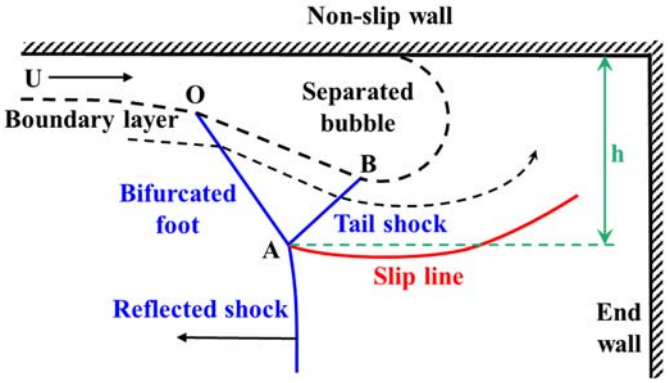

FIG. 1. Schematic of the reflected shock and boundary layer interaction (adapted from [12]).

The interaction between the reflected shock and boundary layer can cause shock bifurcation (e.g., [13-16]) as depicted in Fig. 1. The reflected shock propagates to the left after its collision with the end wall on the right side. A λ-shaped shock structure (see the blue lines in Fig. 1) is formed after the reflected shock and boundary layer interaction.

Due to the advantages of simulations, the complex shock bifurcation has been studied

numerically during the past decades. For examples, Weber et al. [17] performed two-dimensional (2D) simulations of reflected shock and boundary layer interaction, and they examined the sensitivity of the interaction to the Reynolds number, the strength of incident shock and the heat transfer on the wall. Daru et al. [18, 19] conducted high-resolution simulations for the shock bifurcation and found that the Reynolds number affects significantly the location of the triple point and the vortices produced within the lambda shock pattern. Based on the strength of the incident shock, Grogan and Ihme [20] examined three regimes for the reflected shock and boundary layer interaction, including incipient separation, shear layer instability and shock bifurcation. Recently, Chen et al. [21] have assessed the real gas effects on the vortex structure and triple point trajectory using a high-order point-implicit scheme. They found that the triple point trajectory is mainly affected by the shock strength rather than the chemical reaction.

The reflected shock and boundary layer interaction results in a non-uniform flow and temperature distribution behind the reflected shock. Such non-uniformity can induce the local autoignition and thereby affect the accuracy of IDT measurements in shock tube experiments [4, 22]. Strehlow and Cohen [23] found that the reflected shock and boundary layer interaction can cause shock bifurcation and accelerate the reflected shock. The shock bifurcation changes the temperature distribution and induces local autoignition behind the reflected shock. Voevodsky and Soloukhin [24] identified two types of ignition, weak and strong ignition, behind the reflected shock in a stoichiometric hydrogen/oxygen mixture. They found that the boundary between the weak and strong ignition is located around the second explosion limit of hydrogen/oxygen. Meyer and Oppenheim [25] found that weak ignition is related to the sensitivity of ignition delay time, τ_{ig}, to the post-reflected shock temperature, T_5. They proposed a criterion ($\partial\tau_{ig}/\partial T_5 = -2$ μs/K) for the weak-to-strong ignition transition. This relationship was confirmed by other studies including the

simulations. For examples, Yamashita et al. [8] studied numerically and experimentally the ignition kernels appearing behind the reflected shock and proposed a criterion of the induction time gradient to distinguish the near-wall weak ignition from the far-wall strong ignition. Asahara et al. [26] reported that the detached vortices produced by the reflected shock and the boundary layer interaction is one of the key factors for local autoignition. Recently, Grogan and Ihme [5] have found that weak ignition is affected by the boundary conditions on the side wall.

Most studies mentioned above have focused on the structure of fully developed shock bifurcation and the effects of weak ignition on IDT measurement. However, the transient development of the shock bifurcation and the afterwards local ignition kernel is still not well understood. Besides, hydrogen was usually considered in previous numerical studies due to its compact chemical mechanism. There are few studies on other fuels and it is not clear whether weak ignition can be readily triggered by shock bifurcation for fuels other than hydrogen. Therefore, the objectives of this study are to simulate and interpret the formation of shock bifurcation induced by the interaction between the reflected shock and the boundary layer, and to investigate the weak ignition and its transition to strong ignition for different fuels including both hydrogen and dimethyl ether.

II. NUMERICAL MODEL AND SPECIFICATIONS

Two-dimensional simulations considering detailed chemistry and transport are conducted to study the shock bifurcation and non-uniform ignition behind the reflected shock. The transient process is simulated using the parallel block-structured mesh refinement framework AMROC [27-30]. AMROC solves the reactive Navier-Stokes equations for two-dimensional, multi-component, compressible flows using the second-order accurate MUSCL-Hancock finite volume method. A

hybrid Roe-HLL Riemann solver, a conservative second-order accurate central difference scheme and the semi-implicit Runge-Kutta method GRK4A are used to solve the convective fluxes, multi-species diffusion terms and stiff reaction terms, respectively. This efficient and adaptive solver has been extensively validated for ignition and detonation problems (e.g., [5, 20, 28-31]). The details on numerical methods, code validations, and grid convergence can be found in Refs. [27-31]) and thereby are not repeated here.

Two mixtures are considered here: one is stoichiometric hydrogen/oxygen (H_2/O_2) and the other is stoichiometric dimethyl-ether/oxygen (DME/O_2). DME is one of the promising alternative fuels for engines. Unlike hydrogen, DME has a negative temperature coefficient (NTC) with multi-stage ignition behavior. The detailed kinetic model for hydrogen (with 10 species and 21 elementary reactions) [32] and the skeletal kinetic model for DME with low-temperature chemistry (with 39 species and 175 elementary reactions) [33] are used in simulations.

Due to limitations in computational capability, we consider a small rectangular domain of $0 \leq x \leq 7$ or 12 cm and $0 \leq y \leq 0.8$ cm. The computational domain is large enough to ensure the boundary layer growth and its interaction with the reflected shock. The finest mesh size of 3.125 μm and 6.25 μm are used for H_2/O_2 and DME/O_2 mixtures, respectively. This ensures that there are at least 20 grid points per half reaction length for the corresponding ZND structure. Grid convergence is ensured that the mesh resolution is sufficient to resolve the detailed structure of shock bifurcation and local ignition [?]. Besides, it has been shown [?] that the present simulation well captures the reflected shock and boundary layer interaction and λ-shaped shock structure measured by Damazo et al. [?].

The two-dimensional computational domain is $0 \leq x \leq L_x$ and $0 \leq y \leq L_y$. Adiabatic, no-slip boundary conditions are used for the side wall located at $y = L_y = 0.8$ cm and for the end wall

located at $x = L_x = 7$ or 12 cm. Symmetrical boundary conditions are enforced at y=0 cm; and inlet boundary conditions are used at x=0 cm. Initially there is an incident normal shock propagating in the x-direction towards the static H_2/O_2 or DME/O_2 mixture and it reflects on the end wall.

III. RESULTS AND DISCUSSION

A. Reflected shock and boundary layer interaction

In this subsection, we investigate the shock bifurcation caused by the reflected shock and boundary layer interaction in a stoichiometric H_2/O_2 mixture. The temperature and pressure after the reflected shock are 1068 K and 2.8 atm, respectively. The end wall is at $x = L_x = 7$ cm.

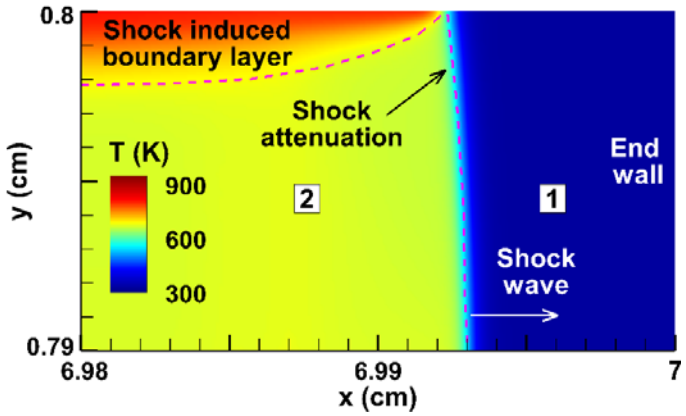

FIG. 2. The temperature contour before the incident shock reflects on the right end wall.

Figure 2 shows the temperature distribution near the boundary layer before the incident shock reflects on the right end wall. The fluid after the incident shock moves to the right side and a thin boundary layer develops on the side wall. Near the boundary shock attenuation occurs and the shock becomes slightly curved as shown in Fig. 2 [21, 34].

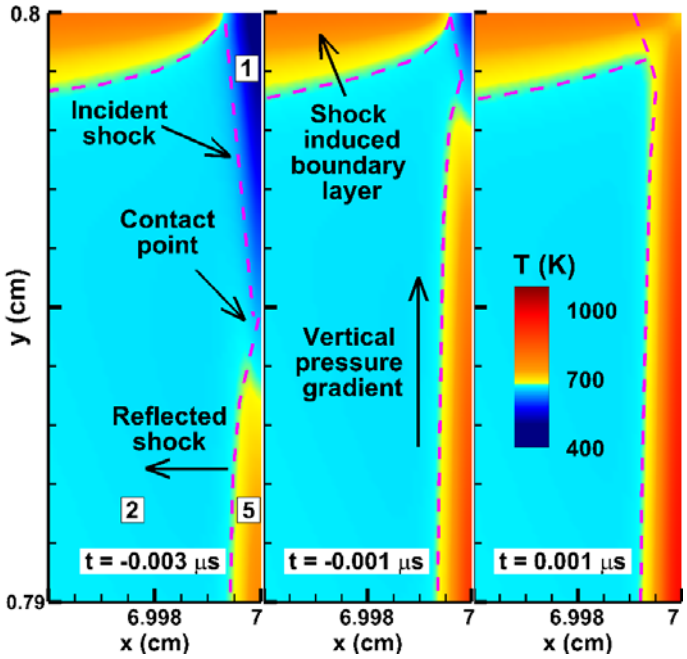

FIG. 3. Evolution of the temperature contour during the asynchronous shock reflection process on the end wall.

The transient evolution of the temperature contour during the asynchronous shock reflection process is shown in Fig. 3. The timing starts (i.e., t=0 μs) when the whole incident shock reflects and leaves the end wall. It is observed that at t=−0.003 μs, the main part of the incident shock reflects at the end wall for y<0.795 cm, which results in rapid increase of the temperature and pressure in region 5. However, due to its curved shape, part of the incident shock near the side wall with y>0.795 cm still propagates toward the end wall. The pressure before the incident shock in region 1 is much lower than that in region 5. Consequently, such asynchronous shock reflection results in a vertical pressure gradient, which drives the fluid to move toward the corner between the end wall and side wall. This was also observed by Chen et al. [21]. After the whole shock reflects on the end wall (i.e., t>0 μs), the vertical pressure gradient still exists since the reflected shock closer to the boundary layer is relatively weaker due to the shock attenuation. Consequently, a wedge-shaped countercurrent flow structure forms as indicated by the streamlines in Fig. 4. In

order to balance the pressure and velocity on both sides of the reflected shock, the wedge-shaped structure gradually evolves into a wedge-shaped oblique shock, which flattens the curved reflected shock front. Such kind of structure evolution was observed before by Davies and Wilson [15].

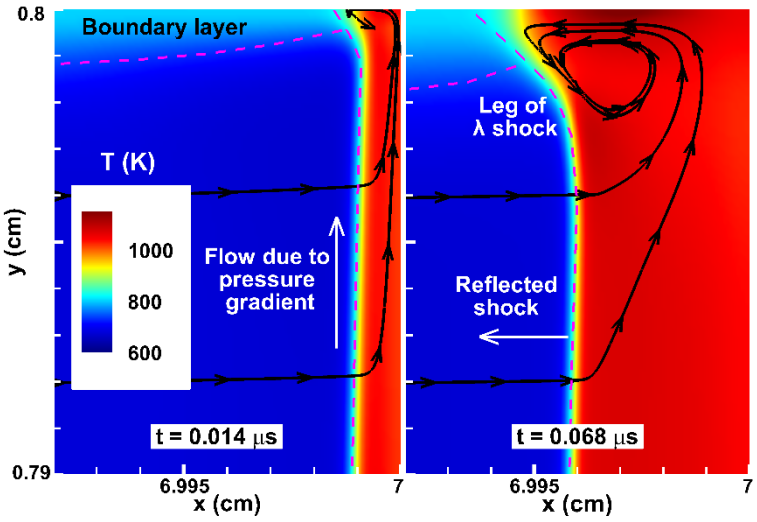

FIG. 4. Evolution of the temperature contour and streamlines in the wedge-shaped oblique shock structure near the boundary layer.

During the propagation of the reflected shock, the stagnation pressure inside the boundary layer is smaller than that behind the reflected shock. The fluid in boundary layer fails to smoothly penetrate into the reflected shock region. Then the boundary layer separates from the wall as shown in Fig. 5. The fluid accumulates around the foot of the bifurcated shock, which results in a reversed flow and stagnation bubble. The size of the bifurcated shock structure and the stagnation bubble grows during the reflected shock propagation. In order to match the pressure difference behind the oblique shock AO and the normal reflected shock AC, another oblique shock AB develops. Consequently, the λ-shaped shock structure appears as shown in Fig. 5. Starting from the triple point A, there is a slip line (indicated by the negative vorticity in Fig. 5) separating the flow compressed by the normal reflected shock AC from that by the oblique shocks AO and AB.

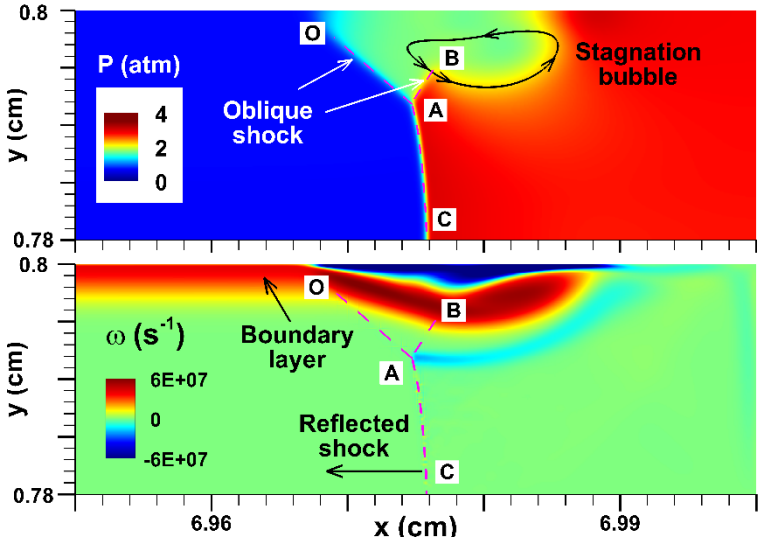

FIG. 5. The pressure and vorticity counter at t=0.418 μs.

The above shock bifurcation inevitably induces a local temperature rise in the flow behind the reflected shock. When the IDT of the H_2/O_2 mixture after the reflected shock is much longer than the duration of the reflected shock propagation, the heat release due to chemical reactions is negligible. Therefore, the local temperature rise can only be caused by the work of pressure and viscous dissipation. To interpret the local temperature rise, we plot in Fig. 6(a) the contour of temperature, absolute value of pressure work and viscous dissipation immediately after the shock reflection (i.e., the reflected shock is very close to the end wall). Figure 6 shows that the temperature after two oblique shocks is smaller than that after the normal reflected shock. This is because the normal reflected shock is much stronger than the oblique shocks. The adverse pressure gradient near the shock bifurcation leads to a reversed flow and the separation of the boundary layer. This results in a large velocity gradient and strong viscous dissipation near the side wall as shown in Fig. 6(a). Near the side wall (region III in Fig. 6a), the pressure work is much smaller than the viscous dissipation. Therefore, it is the viscous dissipation that results in the local temperature rise near the side wall. This is consistent with previous results of Ziegler [31] and

Grogan and Ihme [5]. Figure 6(a) shows that both pressure work and viscous dissipation are very large around the reflected shock (region I). Nevertheless, this only globally increases the temperature in region II and does not induce local temperature rise.

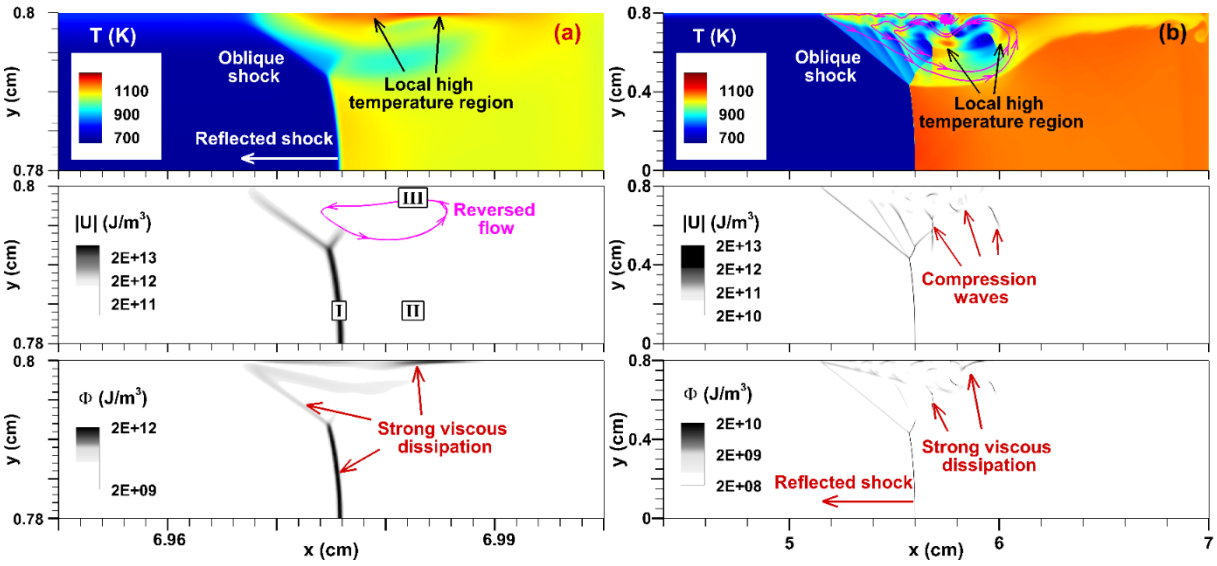

FIG. 6. The contour of temperature, T, absolute value of pressure work , $|U|$, and viscous dissipation, Φ, after shock reflection: (a) t=0.418 μs when the reflected shock is very close to the end wall, and (b) t=23.5 μs when the reflected shock is some distance away from the end wall.

The results for the reflected shock being around 1.4 cm away from the end wall are shown in Fig. 6(b). During the reflected shock propagation, the shock bifurcation gradually grows and more complex flow and shock structure are observed in Fig. 6(b) than in Fig. 6(a). Due to the relative weakness of the oblique shock near the boundary layer, cold fluid before the shocks can be transported to the region after the oblique shocks, resulting in the so-called cold gas contamination [14, 15]. Consequently, some relatively cold regions appear after the oblique shocks as shown in Fig. 6(b). Figure 6(b) indicates that the viscous dissipation is a few orders smaller than the pressure work in the bifurcated region. This is because there are pressure waves produced due to the complex flow and shock interaction. These compression waves collide with one another or with the oblique

shocks, resulting in the local temperature rise. The detached vortexes from the boundary layer transport the mixtures heated by pressure work downstream. Consequently, several ignition kernels with relatively high temperature form around the foot of the bifurcated shock, which induce local weak ignition to be discussed in the next subsection.

In a brief summary, the above results demonstrate that the viscous dissipation and pressure work are the main causes for local temperature rise around the bifurcated shock. The viscous dissipation dominates at the very beginning after the shock reflection, while the pressure work gradually dominates during the subsequent evolution.

B. Weak ignition and its transition to strong ignition

In this subsection, we study the weak ignition and its transition to strong ignition as the post-reflected shock temperature increases. The post-reflected shock pressure is fixed to be P_5=2.8 atm. The stoichiometric H_2/O_2 mixture is considered and the end wall is at x=7 cm.

For a relatively low post-reflected shock temperature of T_5=1068 K, the transient evolution of temperature distribution is shown in Fig. 7.

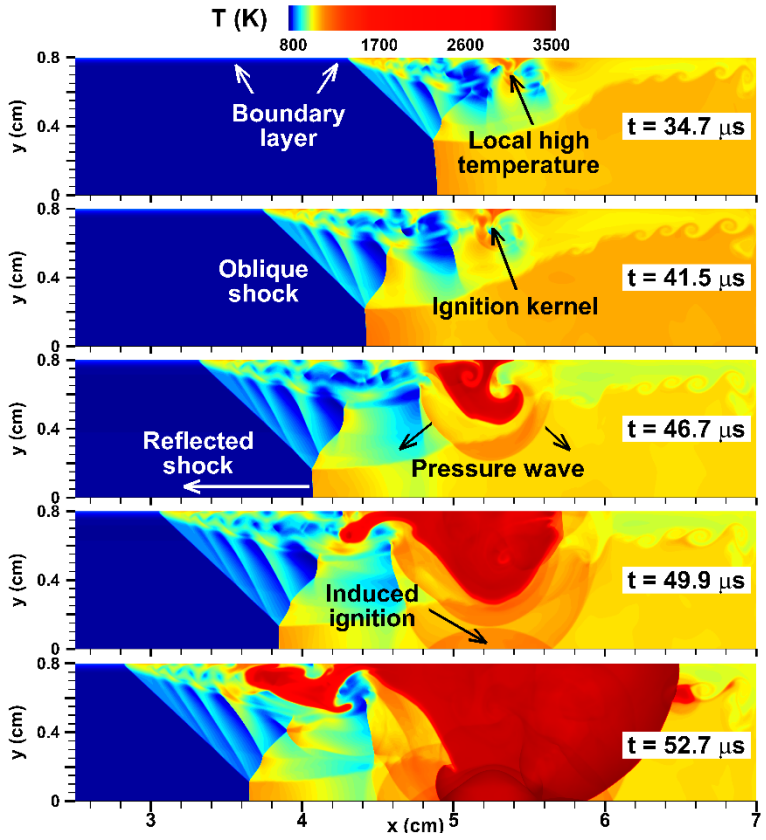

FIG. 7. The evolution of temperature contour during the weak ignition process for T_5=1068 K.

At t=34.7 μs, several regions with local high temperature are shown to appear at the foot of bifurcated shock due to the viscous dissipation and pressure work discussed in the previous subsection. The local high temperature triggers chemical reactions in the H_2/O_2 mixture and induces local ignition in the stagnation region of bifurcated shock around t=41.5 μs. Ignition first occurs at some distance away from the reflecting end wall. This is the so-called "weak ignition" phenomenon [24]. The ignition kernel expands and the local heat release produces pressure waves which compress the unburned mixture. Consequently, several ignition kernels are induced at the central region around t=49.9 μs. Finally, the whole mixture behind the reflected shock ignites. Therefore, the local ignition is mainly induced by the reflected shock and boundary layer interaction under this relatively low post-reflected shock temperature.

Then we increase the post-reflected shock temperature to T_5=1073 K while keeping the pressure to be around P_5=2.8 atm. The results are shown in Fig. 8.

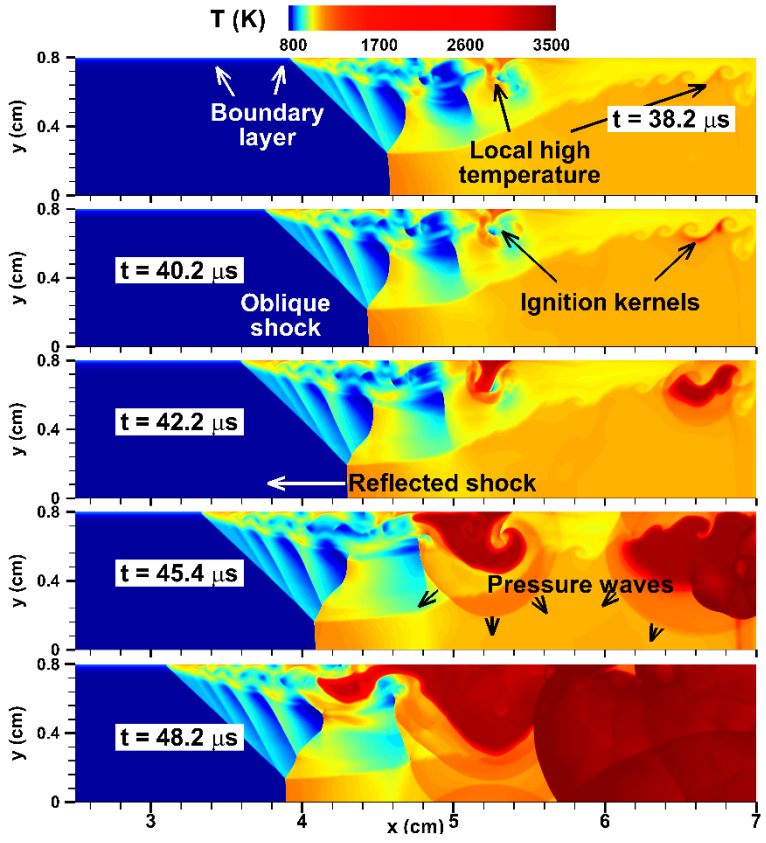

FIG. 8. The evolution of temperature contour during the ignition process for T_5=1073 K.

Figure 8 shows that the local high temperature appears not only in the stagnation region of bifurcated shock but also around the slip line close to the end wall. The slip line represents a thin vorticity layer, which is extremely unstable during the shock bifurcation and it curls and rolls up [8, 17, 26, 35, 36]. A vortex circle is observed near the corner between the end wall and side wall, which has relatively high temperature and reactivity. Since the mixture around the corner is first compressed by the reflected shock, it ignites earlier than the surrounding mixture. Consequently, two ignition kernels, one at the foot of bifurcated shock and the other close to the end wall, simultaneously appear at t=40.2 μs, as shown in Fig. 8. These two ignition kernels propagate

outwardly and produce pressure waves which compress the unburned mixture. Finally, a detonation develops near the end wall due to the coherent coupling between ignition and pressure wave, which can be explained by the SWACER (Shock Wave Amplification by Coherent Energy Release) mechanism [5, 37, 38]. During this ignition process, both weak ignition at the foot of bifurcated shock and strong ignition near the end wall happen. Therefore, it is a transition from pure weak ignition to pure strong ignition. The local ignition behaviors are mainly induced by the reflected shock and boundary layer interaction and the non-uniformities of flow near the end wall.

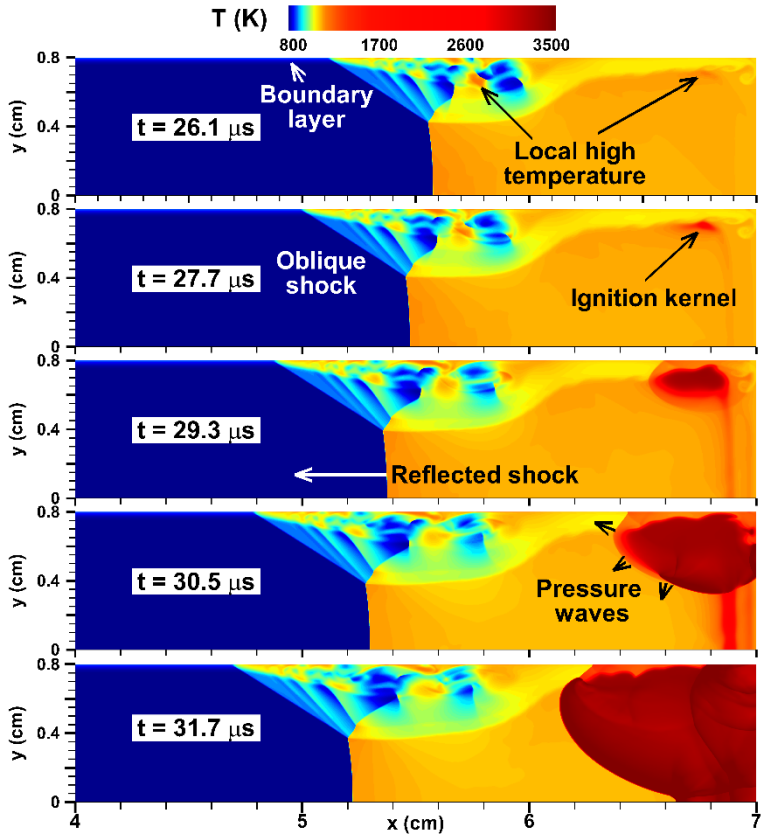

FIG. 9. The evolution of temperature contour during the ignition process for T_5=1091 K.

When the post-reflected shock temperature is further increased to T_5=1091 K, transition to strong ignition is observed as shown in Fig. 9. The higher post-reflected shock temperature results in shorter ignition delay time for the mixture first compressed by the reflected shock. Though

several hot spots with relatively high temperature are formed at the foot of the bifurcated shock, its temperature is lower than that near the end wall. Consequently, the mixture closer to the corner ignites first. Meanwhile, the mixture close to the end wall and at the central region also ignites spontaneously due to its high reactivity. These two ignition regions merge with each other, resulting in global ignition of the mixture behind the reflected shock. Similar phenomena were also observed by Knisely et al. [36] and Asahara et al. [26].

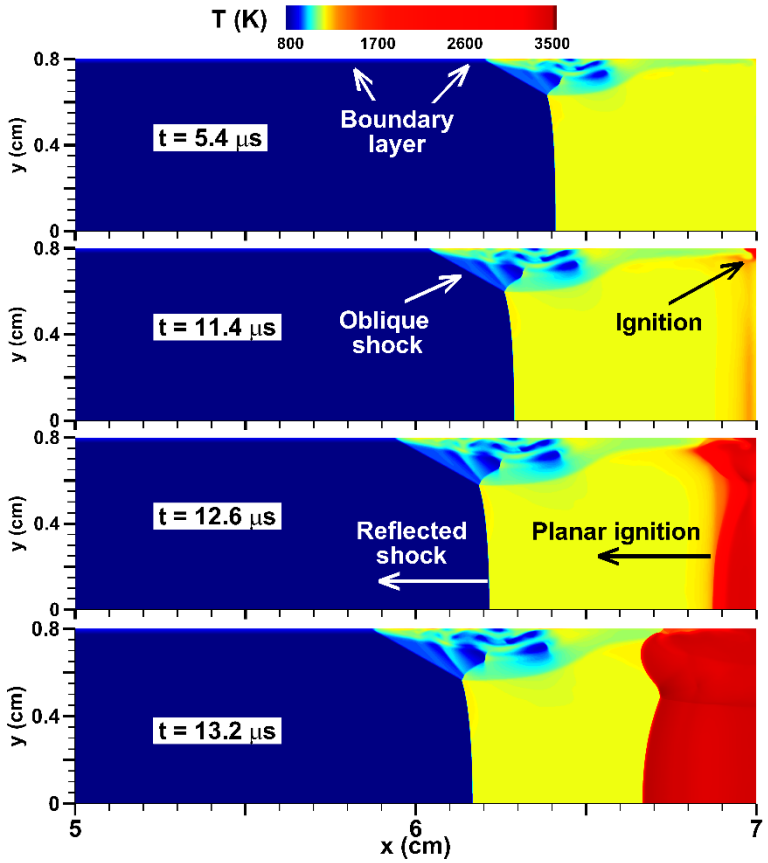

FIG. 10. The evolution of temperature contour during the ignition process for T_5=1146 K.

Finally, the post-reflected shock temperature is further increased to T_5=1146 K and Fig. 10 shows that the ignition first occurs near the end wall. A nearly planar ignition front quickly consumes the H_2/O_2 mixture compressed by the reflected shock. The ignition front propagates very fast so that it can be approximated as a homogeneous ignition process.

Figures 7-10 indicate that with the increase of the post-reflected shock temperature, the ignition behavior gradually transits from the weak ignition at the foot of bifurcated shock to the strong ignition starting from the end wall.

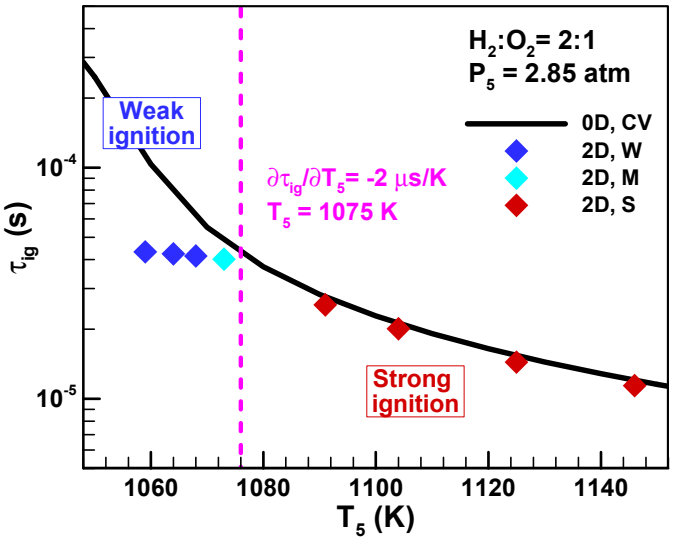

FIG. 11. Comparison of ignition delay time from 2D simulations and 0D constant-volume (CV) homogeneous ignition for a stoichiometric H_2/O_2 mixture at P_5=2.85 atm. W and S represent weak and strong ignition, respectively, and M denotes the mixed mode of weak and strong ignition.

Figure 11 compares the IDT recorded in 2D simulations with that predicted by 0D constant-volume homogeneous ignition. For strong ignition, very good agreement between 2D and 0D results is achieved. However, at relatively low post-reflected shock temperature, weak ignition happens and the IDT from 2D simulations is much smaller than that that from 0D simulations. This is because the local hot spot and ignition around the foot of the shock bifurcation accelerates the global ignition behind the reflected shock. Therefore, the occurrence of weak ignition has a great impact on the IDT measurement in shock tube experiments.

The sensitivity of IDT to the post-reflected shock temperature has been used in previous

studies as a criterion to distinguish the weak ignition from strong ignition. Based on experimental and numerical results for stoichiometric H_2/O_2 mixtures, Meyer and Oppenheim [25] proposed the critical value of $\partial \tau_{ig}/\partial T_5$=-2 μs/K for the strong ignition limit. We also examine this ignition criterion through simulations and compare to results of other studies [5, 25], which is shown in Fig. 12.

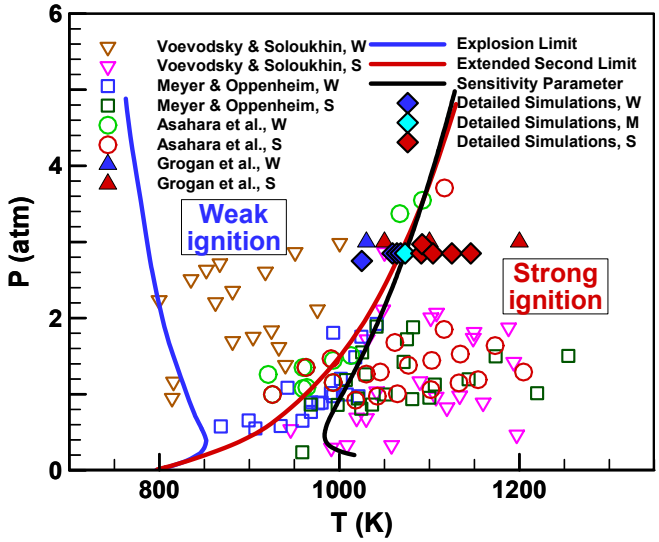

FIG. 12. Explosion limit (blue line), extended second limit (red line) and the sensitivity parameter of $\partial \tau_{ig}/\partial T_5$=-2 μs/K (black line) in the plot of pressure versus temperature for a stoichiometric H_2/O_2 mixture. The open symbols represent experimental results from the literature, and the closed symbols represent simulation results from Grogan and Ihme [5] (triangles) and this work (diamonds). W and S represent weak and strong ignition, respectively, and M denotes the mixed mode of weak and strong ignition.

It is seen that the sensitivity criteria of Meyer and Oppenheim [25] well represents the boundary between weak and strong ignition for the stoichiometric H_2/O_2 mixture. Since ignition is more sensitive to temperature changes at larger absolute values of the sensitivity, $|\partial \tau_{ig}/\partial T_5|$, the local high temperature kernels induced by the reflected shock and boundary interaction can easily trigger

local weak ignition behind the reflected shock. Therefore, weak ignition occurs under relatively high sensitivity conditions as shown in Fig. 12. At relative high temperature, the sensitivity, $|\partial\tau_{ig}/\partial T_5|$, becomes small and thereby strong ignition is observed as shown in Fig. 12.

Though the sensitivity, $\partial\tau_{ig}/\partial T_5$, predicts the boundary between weak and strong ignition well, it does not take into account the IDT. With the increase of the IDT, the interaction between the reflected shock and boundary layer becomes longer and thereby the size of the bifurcated shock becomes larger, which results in more cold gas contamination and stronger mixing. This might prevent the formation of local high temperature spots and thereby inhibit the local weak ignition. Consequently, a shorter IDT might be helpful for the appearance of weak ignition. To take into account this fact, we propose to use the relative sensitivity, $(\partial\tau_{ig}/\partial T_5)/\tau_{ig}$ or $\partial\ln\tau_{ig}/\partial T_5$, to characterize the condition for weak ignition. The increase of $\partial\tau_{ig}/\partial T_5$ and the decease of τ_{ig} both help to induce the weak ignition.

Figure 13 shows the IDT, sensitivity and relative sensitivity of IDT to the post-reflected shock temperature for a stoichiometric H_2/O_2 mixture. The IDT and sensitivity both decrease exponentially with the temperature when the temperature is within certain range. At low temperature, the relative sensitivity, $\partial\ln\tau_{ig}/\partial T_5$, reaches its peak value, and thereby the local high temperature spots can readily induce weak ignition. Though the sensitivity, $\partial\tau_{ig}/\partial T_5$, can effectively distinguish the weak and strong for a stoichiometric H_2/O_2 mixture, the relative sensitivity, $\partial\ln\tau_{ig}/\partial T_5$, needs to be introduced for other fuels, especially for fuels with long IDT. It is noted that the sensitivity analysis of IDT is used to qualitatively characterize the ignition mode behind the reflected shock. The details on the local ignition behavior are mainly determined by the non-uniformity of the flow.

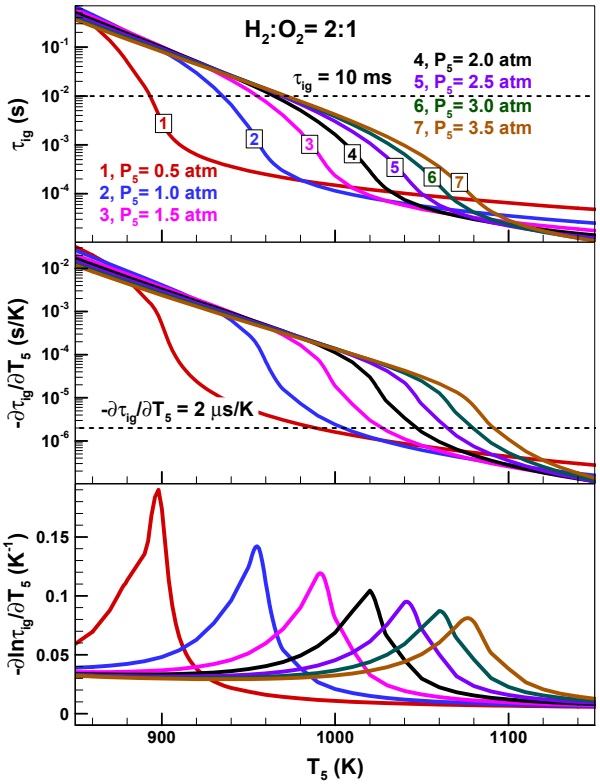

FIG. 13. Change of the ignition delay time, the sensitivity and the relative sensitivity of ignition delay to the post-reflected shock temperature for a stoichiometric H_2/O_2 mixture at different pressures.

C. Results for DME/O_2 mixtures

In this subsection the ignition of the stoichiometric DME/air mixture is considered. First, its IDT and its sensitivity and relative sensitivity are shown in Fig. 14. Since the logarithmic scale is used for the sensitivity, only the positive value of $(-\partial\tau_{ig}/\partial T_5)$ is shown. Figure 14 shows that the IDT changes non-monotonically with the temperature and the NTC behavior appears within a certain temperature range. Around the NTC region, the sensitivity, $-\partial\tau_{ig}/\partial T_0$, becomes negative or close to zero. Consequently, a small temperature rise due to shock bifurcation cannot induce local ignition. Besides, the relative sensitivity, $-\partial\ln\tau_{ig}/\partial T_0$, for DME/$O_2$ is much smaller than that for H_2/O_2. Therefore, it is more difficult to achieve weak ignition in the DME/O_2 mixture than in the

H_2/O_2 mixture.

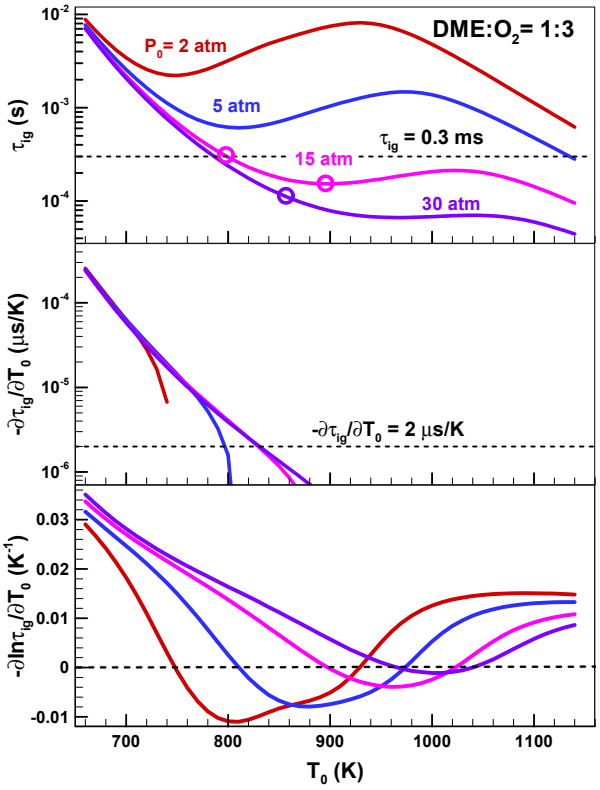

FIG. 14. Change of the ignition delay time, the sensitivity and the relative sensitivity of ignition delay to the post-reflected shock temperature for a stoichiometric DME/O_2 mixture at different pressures.

To show the validity of the above conclusion, we conduct 2D simulations considering detailed chemistry and transport for a stoichiometric DME/O_2 mixture under low post-shock temperature condition. Three cases corresponding to the open circles in Fig. 14(a) are considered. The results for the case of T_5=797 K and P_5=15 atm are shown in Fig. 15. In Fig. 15(a), several spots with local high temperature are observed around the foot of the bifurcation at t=54.6 μs. As discussed before, such local high temperature is caused by the strong viscous dissipation and pressure work during the reflected shock and boundary layer interaction. Since the IDT corresponding to the highest temperature in these hot spots is still relatively long, no local ignition

is observed. The vortexes originating from the boundary layer detach and move downstream carrying the mixture with relatively high temperature, which gradually dissipates in the main flow by strong mixing. This further prevents the local ignition in these hot spots.

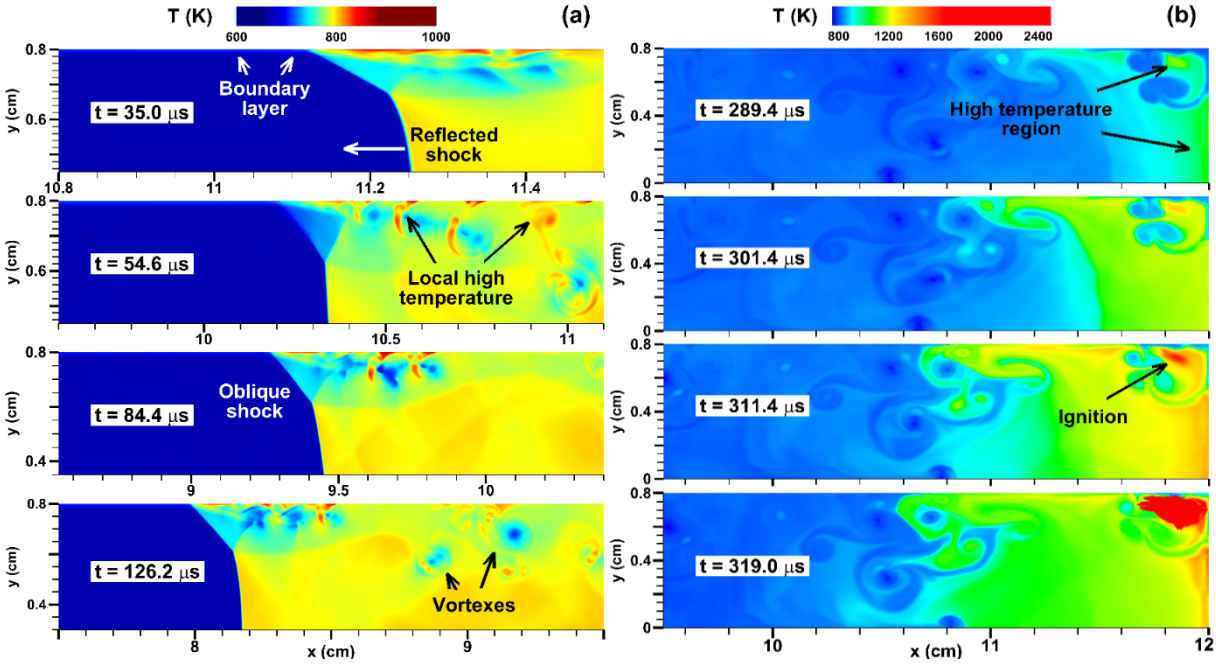

FIG. 15. The evolution of temperature contour during the ignition process for a stoichiometric DME/O_2 mixture with T_5=797 K and P_5=15 atm: (a) reflected shock and boundary layer interaction, (b) strong ignition process.

On the other hand, compared to the mixture far away from the end wall, the mixture near the end wall is compressed earlier by the reflected shock. This makes the ignition to first occur near the corner between end wall and side wall around t=311.4 μs as shown in Fig. 15(b). This eventually induces strong ignition behind the reflected shock. For the other two cases with (T_5=895 K and P_5=15 atm) and (T_5=855 K and P_5=30 atm) marked in Fig. 14(a), strong ignition is also observed. Therefore, compared to the H_2/O_2 mixture, it is much more difficult to achieve weak ignition in the DME/O_2 mixture.

IV. CONCLUSIONS

Two-dimensional transient simulations are conducted for shock bifurcation and local ignition induced by the interaction between the reflected shock and the boundary layer. Both stoichiometric H_2/O_2 and DME/O_2 mixtures are considered. Detailed chemistry and transport are included in simulations which use block-structured adaptive mesh refinement to efficiently resolve the reflected shock and the boundary layer interaction. The main conclusions are:

(1) The formation and evolution of shock bifurcation are analyzed. It is demonstrated that the viscous dissipation and pressure work are the main causes for local temperature rise around the bifurcated shock. The viscous dissipation dominates at the very beginning after the shock reflection, while the pressure work gradually dominates during the subsequent evolution.

(2) Local ignition happens at these hot spots, which results in non-uniform ignition after the reflected shock and weak ignition. With the increase of the post-reflected shock temperature, there is gradual transition from weak ignition (occurring at the foot of bifurcated shock due to the reflected shock and boundary layer interaction) to strong ignition occurring near the end wall. A mixed mode of weak and strong ignition is identified in this work.

(3) Though the sensitivity, $\partial\tau_{ig}/\partial T_5$, can effectively distinguish the weak and strong for a stoichiometric H_2/O_2 mixture, the relative sensitivity, $\partial \ln\tau_{ig}/\partial T_5$, needs to be introduced for other fuels with long ignition delay time. Compared to the H_2/O_2 mixture, it is much more difficult to achieve weak ignition in the DME/O_2 mixture which has a relatively longer ignition delay time and smaller relative sensitivity.

ACKNOWLEDGMENTS

This work was supported by the National Natural Science Foundation of China (Nos. 51861135309 and 91841302). We thank Prof. Shengkai Wang at Peking University, Dr. Song Chen at Technische Universität München and Dr. Wang Han at University of Edinburgh for helpful discussion.

---

[1] R. K. Hanson, D. F. Davidson, Recent advances in laser absorption and shock tube methods for studies of combustion chemistry, Progress in Energy and Combustion Science **44**, 103 (2014).

[2] N. Chaumeix, B. Imbert, L. Catoire, and C.-E. Paillard, The onset of detonation behind shock waves of moderate intensity in gas phase, Combustion Science and Technology **186**, 607 (2014).

[3] G. A. Pang, D. F. Davidson, and R. K. Hanson, Experimental study and modeling of shock tube ignition delay times for hydrogen-oxygen-argon mixtures at low temperatures, Proceedings of the Combustion Institute **32**, 181 (2009).

[4] E. L. Petersen, R. K. Hanson, Nonideal effects behind reflected shock waves in a high-pressure shock tube, Shock Waves **10**, 405 (2001).

[5] K. P. Grogan, M. Ihme, Weak and strong ignition of hydrogen/oxygen mixtures in shock-tube systems, Proceedings of the Combustion Institute **35**, 2181 (2015).

[6] J. T. Lipkowicz, I. Wlokas, and A. M. Kempf, Analysis of mild ignition in a shock tube using a highly resolved 3D-LES and high-order shock-capturing schemes, Shock Waves **29**, 511 (2019).

[7] C. Huang, C. Qi, and Z. Chen, Non-uniform ignition behind a reflected shock and its influence on ignition delay measured in a shock tube, Shock Waves **29**, 957 (2019).

[8] H. Yamashita, J. Kasahara, Y. Sugiyama, and A. Matsuo, Visualization study of ignition modes behind bifurcated-reflected shock waves, Combustion and Flame **159**, 2954 (2012).

[9] Y. Uygun, S. Ishihara, and H. Olivier, A high pressure ignition delay time study of 2-methylfuran and tetrahydrofuran in shock tubes, Combustion and Flame **161**, 2519 (2014).

[10] T. Javed, J. Badra, M. Jaasim, E. Es-Sebbar, M. F. Labastida, S. H. Chung, H. G. Im, and A. Farooq, Shock Tube Ignition Delay Data Affected by Localized Ignition Phenomena, Combustion Science and Technology **189**, 1138 (2017).

[11] E. Ninnemann, B. Koroglu, O. Pryor, S. Barak, L. Nash, Z. Loparo, J. Sosa, K. Ahmed, and S. Vasu, New insights into the shock tube ignition of H2/O2 at low to moderate temperatures using high-speed end-wall imaging, Combustion and Flame **187**, 11 (2018).

[12] K. Matsuo, S. Kawagoe, and K. Kage, The interaction of a reflected shock wave with the boundary layer in a shock tube, Bulletin of JSME **17**, 1039 (1974).

[13] H. Mark, The interaction of a reflected shock wave with the boundary layer in a shock tube, Technical Report TM-1418, NACA (1958).

[14] L. Davies, The Interaction of the Reflected Shock with the Boundary Layer in a Shock Tube and its Influence on the Duration of Hot Flow in the Reflected-Shock Tunnel. Part I, Aerodynamics Division, Nationlal Physical Laboratory, England, 1965.
[15] L. Davies, J. Wilson, Influence of Reflected Shock and Boundary-Layer Interaction on Shock-Tube Flows, Physics of Fluids **12**, 37 (1969).
[16] H. Kleine, V. Lyakhov, L. Gvozdeva, and H. Grönig, Bifurcation of a reflected shock wave in a shock tube, Shock Waves 261 (1992).
[17] Y. S. Weber, E. S. Oran, J. P. Boris, and J. D. Anderson, The numerical simulation of shock bifurcation near the end wall of a shock tube, Physics of Fluids **7**, 2475 (1995).
[18] V. Daru, C. Tenaud, Evaluation of TVD high resolution schemes for unsteady viscous shocked flows, Computers & Fluids **30**, 89 (2001).
[19] V. Daru, C. Tenaud, Numerical simulation of the viscous shock tube problem by using a high resolution monotonicity-preserving scheme, Computers & Fluids **38**, 664 (2009).
[20] K. P. Grogan, M. Ihme, Regimes describing shock boundary layer interaction and ignition in shock tubes, Proceedings of the Combustion Institute **36**, 2927 (2017).
[21] S. Chen, Q. Sun, I. Klioutchnikov, and H. Olivier, Numerical study of chemically reacting flow in a shock tube using a high-order point-implicit scheme, Computers & Fluids **184**, 107 (2019).
[22] E. L. Petersen, R. K. Hanson, Measurement of reflected-shock bifurcation over a wide range of gas composition and pressure, Shock Waves **15**, 333 (2006).
[23] R. A. Strehlow, A. Cohen, Limitations of the Reflected Shock Technique for Studying Fast Chemical Reactions and Its Application to the Observation of Relaxation in Nitrogen and Oxygen, Journal of Chemical Physics **30**, 257 (1959).
[24] V. V. Voevodsky, R. I. Soloukhin, On the mechanism and explosion limits of hydrogen-oxygen chain self-ignition in shock waves, Symposium (International) on Combustion **10**, 279 (1965).
[25] J. Meyer, A. Oppenheim, On the shock-induced ignition of explosive gases, Symposium on Combustion **13**, 1153 (1971).
[26] M. Asahara, Y. Shirakawa, A. Hayashi, and N. Tsuboi, Strong and mild ignition mechanism behind reflected shock wavea in hydrogen mixture, International Conference on Hydrogen Safety, 2013.
[27] R. Deiterding, Parallel adaptive simulation of multi-dimensional detonation structures, Brandenburgischen Technischen Universitat Cottbus, 2003.
[28] R. Deiterding, A parallel adaptive method for simulating shock-induced combustion with detailed chemical kinetics in complex domains, Computers & Structures **87**, 769 (2009).
[29] R. Deiterding, Block-structured adaptive mesh refinement-theory, implementation and application, Esaim: Proceedings **34**, 97 (2011).
[30] R. Deiterding, High-resolution numerical simulation and analysis of Mach reflection structures in detonation waves in low-pressure H2-O2-Ar mixtures: a summary of results obtained with the adaptive mesh refinement framework AMROC, Journal of Combustion **2011**, 1 (2011).
[31] J. L. Ziegler, Simulations of compressible, diffusive, reactive flows with detailed chemistry using a high-order hybrid WENO-CD scheme, California Institute of Technology, 2012.
[32] J. Li, Z. Zhao, K. Andrei, and F. L. Dryer, An updated comprehensive kinetic model of hydrogen combustion, International Journal of Chemical Kinetics **36**, 566 (2004).
[33] A. Bhagatwala, Z. Luo, H. Shen, J. A. Sutton, T. Lu, and J. H. Chen, Numerical and experimental investigation of turbulent DME jet flames, Proceedings of the Combustion

Institute **35**, 1157 (2015).
[34] A. Deshpande, B. Puranik, Effect of viscosity and wall heat conduction on shock attenuation in narrow channels, Shock Waves **26**, 1 (2016).
[35] G. Wilson, S. Sharma, and W. Gillespie, Time-dependent simulation of reflected-shock/boundary layer interaction, 31st Aerospace Sciences Meeting, 1993.
[36] A. Knisely, J. M. Austin, C. Bacon, and A. Khokhlov, Strong and Weak Ignition in 2H2 + O2 behind Reflected Shocks in Two-Dimensional Navier-Stokes Simulations with Detailed Chemistry, 29th International Symposium on Shock Waves, 2013.
[37] J. H. Lee, R. Knystautas, and N. Yoshikawa, Photochemical initiation of gaseous detonations, Acta Astronautica **5**, 971 (1978).
[38] R. Blumenthal, K. Fieweger, K. Komp, and G. Adomeit, Gas dynamic features of self ignition of non diluted fuel/air mixtures at high pressure, Combustion science and technology **113**, 137 (1996).